ACS Photonics

Article

pubs.acs.org/journal/apchd5

Comparative Study of Plasmonic Colors from All-Metal Structures of Posts and Pits

Xiao Ming Goh,[†] Ray Jia Hong Ng,[‡] Sihao Wang,[†] Shawn J. Tan,[†] and Joel K.W. Yang*[,†,‡]

[†]Institute of Materials Research and Engineering, A*STAR (Agency for Science, Technology and Research), 2 Fusionopolis Way, #08-03, Innovis, Singapore 138634, Singapore

[‡]Singapore University of Technology and Design, 8 Somapah Road, Singapore 487372, Singapore

ABSTRACT: Thin-film and isolated metal nanostructures with localized plasmon resonances in the visible spectrum are promising for commercial adoption of ultrahigh resolution color printing. As metallization processes used in printing industries tend to produce thick and continuous metal coatings, challenges remain in designing structures with similar local resonances to produce colors. Here, we demonstrate color elements through surface textures on an encapsulated silver surface thus bringing plasmonic colors a step closer to commercial printing processes. We probe the chromatic range of protrusions and indentations, two possible architectures that could form on an all-metal surface, and further investigate the modulation of color when the protrusions evolve into the reversed structures of indentations. Notably, the indentations generate pitch-dependent colors; albeit protrusions generate size-dependent colors that are superior. Building upon this blueprint for all-metal plasmonic color printing, we highlight the spectral tunability of these complementary geometries through an oxidation-robust color microprint. We envision that these structures will enable economically feasible ultrahigh resolution color creation with metallic finishes on plastic films.

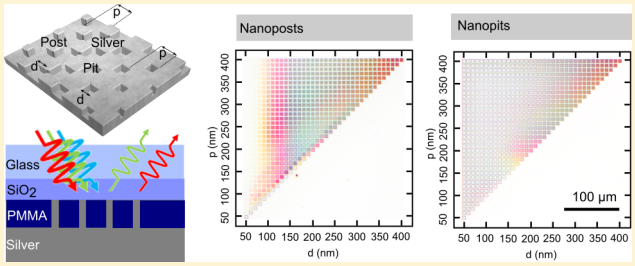

KEYWORDS: *nanoplasmonics, color printing, high-resolution, nanoantenna, electron-beam lithography*

Nanoparticle plasmon resonators enhance and confine electromagnetic fields in subdiffraction-limited volumes at the nanoscale and are poised for development into the next-generation of optoelectronic devices, ultrasensitive detectors and color displays. An essential advantage of metal nanostructures toward this advancement lies in the ability to easily tailor their absorption and scattering profiles in the visible light regime simply by altering the nanostructure size, shape or material.[1] For example, plasmonic nanostructures as color elements offer accessible spectral tuning in the form of highly transmissive filters[2−9] or ultrahigh resolution reflective pixels.[10−15] Such approaches provide a highly tunable, dye-free, fade-free alternative to conventional pigment-based color printing.[10−15] Multiple levels of information can further be encoded into a single area by tailoring the nanostructure polarization response,[2,12,16] providing an additional level of complexity that is attractive for engineering antiforgery safeguards.[1] Discrete metal resonator arrays with distinct plasmon resonances, either metallic elements such as disks[11,13,14] or rods[17,18] that are isolated from each other and surrounded by dielectric, or patterns of slots[3−6,19,20] or holes[2,21] perforated in metallic thin films, are well-established plasmonic color geometries. Vacuum-based electron-beam evaporation processes that afford a directional line-of-sight deposition are frequently employed to form nanostructures, producing isolated metal antennas[10−14,17] atop nanoposts with uncoated vertical sidewalls.[10−13] The functionalities of such architectures hinge on their well-defined metal thicknesses, typically in the order of tens of nanometers (~20 nm), easily achieved using cleanroom techniques.

A steep barrier-of-entry, however, exists for adopting isolated metal resonators into the printing industry, as cleanroom processes are expensive compared to industrial metallization. It should be noted that the use of roll-to-roll patterning[22,23] is a cost-effective, upscalable to mass production industry standard that has been demonstrated for plasmonic structural colors[24−26] in tandem with metal evaporation. Regardless, in the industry, metals are normally deposited without vacuum or the precision in thickness available through cleanroom processes, forming connected metal structures, rather than the widely demonstrated isolated structures coated by thin metal films.[10−14,17] For example, processes such as spray deposition[27] or gravure printing[28] produce a continuous micron-thick metal film that covers the prepatterned substrate. The main challenge in the burgeoning field of plasmonic colors thus lies in bridging the technological gap between cleanroom and standard commercial processes employed for achieving cost-effective, scalable nanopixels. The ability to pattern colors into bulk metals without requiring costly vacuum-based processes will facilitate integration of plasmonic colors into standard industry printing techniques. Moreover, investigations into color generation in

Received: February 12, 2016
Published: May 11, 2016

DOI: 10.1021/acsphotonics.6b00099
ACS Photonics 2016, 3, 1000−1009

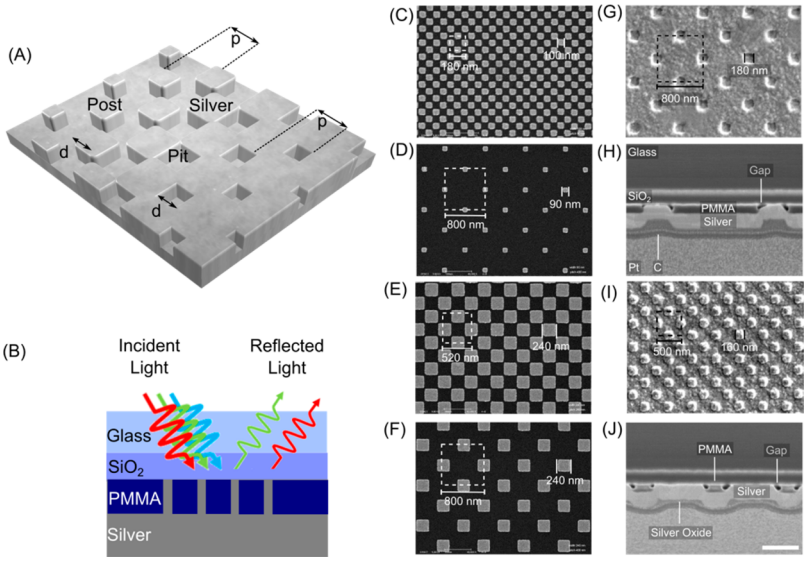

Figure 1. Schematic of plasmonic color elements formed on an all-metal surface comprising square-shaped nanoposts that evolve into nanopits. (a) White light interaction with an all-metal structure, where distinct wavelengths of light are scattered back as different colors tuned by the nanostructure size. Color information is encoded in the width *d* of the square features with pixel pitch *p*. (b) Nanoposts and nanopits are formed by spin-coating a 80 nm thick layer of PMMA and patterned using electron beam lithography (EBL). A 1 nm thick layer of chromium was deposited between the SiO_2 and glass layers to avoid sample charging during EBL. After resist development, the patterned structures are coated with a 200 nm thick layer of silver and inverted for imaging as indicated. SEM images of test samples for the nanoposts are shown in (c−f). Note that the structures imaged here are 30 nm tall nanoposts made by e-beam evaporation of 1 nm thick chromium and 30 nm thick gold, followed by the process of lift-off. The encapsulated structures shown in (b) would otherwise inhibit imaging. SEM images of the top views (g, i) and cross-section profiles (h, j) of nanopost and nanopits. Scale bar: 250 nm.

optically thick metal layers (>200 nm) or on continuous metal films are scant.[19,29] For example, in the extreme case where the metal gets thick and opaque, it is not well-studied whether nanotextured surfaces on a bulk piece of metal would generate a broad range of colors.

A fundamental consideration in generating plasmonic colors is the dielectric constant of the metals in the visible wavelength range. Loss mechanisms such as interband transitions and scattering can be significant and limit the palette of available colors.[1] For example, gold suffers from high loss in the blue wavelength range; aluminum exhibits low losses in the blue and ultraviolet but is lossy in the infrared regime (>800 nm).[29,30] To gain relevance in consumer products, however, practical issues of economic viability through cheaper materials, as well as forming large areas of robust color elements cheaply are equally important. The resistivity of the metal against chemical reactions to preserve colors is also crucial. For example, gold, with or without a protective coating,[14] is inherently robust against corrosion, but is very costly. Silver produces a broader basic color palette than aluminum,[10] but is susceptible to oxidation[31] or sulphidation[32] under ambient conditions. Thus, far, the effect of sulphidation on plasmonic-generated color has yet to be thoroughly investigated or reported. Here, we address some of the aforementioned challenges stymying the development of plasmonic color printing toward industry-compatible process and applications.

In our previous works, discrete, heterogeneous metallic nanostructures such as gold/silver[11] and aluminum,[10,12] formed on patterned dielectric nanoposts, were employed as ultrahigh resolution plasmonic color elements.[10−12] More recently, we showed theoretically, the possibility of producing localized plasmon resonances in an all-metallic substrate.[33] Nanometric protrusions on a bulk metal layer can be designed to exhibit a large absorption in the visible spectrum, representative of a saturated subtractive color. Building upon our previous works, here we demonstrate a scalable strategy that employs solid metal nanostructures to produce a full range of plasmonic colors in reflection mode. The processes for forming these structures are not only compatible with existing industry metallization processes, they also provide an excellent platform for studying the spectral tunability of solid metal nanostructures and elucidate the physics underpinning color generation on all-metallic surfaces. To this end, we study color elements of connected arrays comprising square-shaped protrusions or indentations (Figure 1a) formed in optically thick metal films. The color shifts produced as the metal nanoposts evolve into the reversed structure of nanopits, and the evolution of colors as the metal layer is increased from a thin (∼20 nm) film to an optically opaque (∼200 nm) film are also investigated. Additionally, we report novel results showing the controlled color degradation in silver nanostructures over time, with an attempt at circumventing it.

To systematically probe the chromatic range of these color elements, we examine the modulation afforded by color palettes comprising arrays of square-shaped nanostructures laid out in a checkerboard pattern. The pixel pitch *p*, and width of the squares *d*, were varied in a manner such that protrusions evolve into reversed structures of indentations with increasing pitch and widths. Arrays of square-shaped nanoposts with a height of ∼80 nm were patterned in Poly(methyl methacrylate) (PMMA), a positive-tone resist using EBL as detailed in Methods. A 200 nm thick layer of silver was subsequently deposited onto the prepatterned transparent Corning glass substrate using electron beam evaporation. These steps yielded an optically opaque metal film patterned with arrays of nanometric protrusions and indentations at the interface between the metal and the glass substrate, that is, posts and pits, as illustrated in Figure 1a,b. Note that the nanopits

DOI: 10.1021/acsphotonics.6b00099
ACS Photonics 2016, 3, 1000−1009

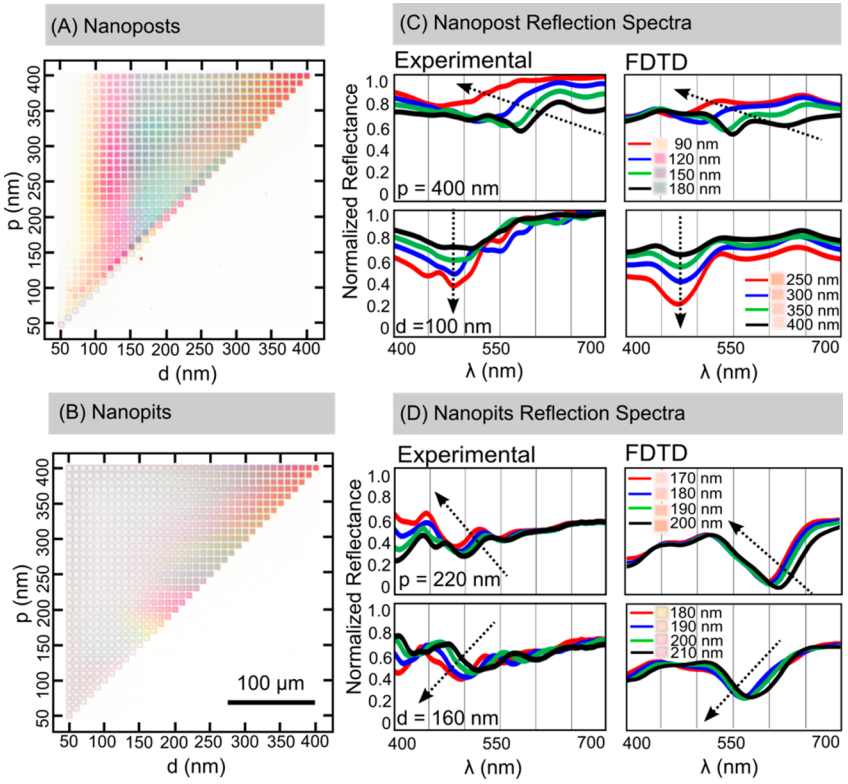

Figure 2. Bright-field optical micrographs and spectral analyses for connected arrays of nanoposts and nanopits with varying lateral dimensions formed in a 200 nm thick metal film. Optical images of color palettes for (a) nanoposts and (b) nanopits under normal illumination. Each 10 μm × 10 μm pixel array was spaced 2 μm away from the neighboring pixel. Pixel diameter and pitch were varied from 50−400 nm in 10 nm increments in the *y*- and *x*-axes, respectively. Measured and simulated reflection spectra for (c) nanoposts and (d) nanopits under normal illumination. Arrows indicate decreasing dimension and pitch sizes.

penetrate only partway through the metal film to form indentations rather than completely through the metal film as in a true hole-aperture. Plasmon resonances elicited will manifest as different colors under bright-field microscopy when the sample is illuminated through the glass, as indicated in Figure 1b.

It should be noted that the nanostructures imaged in Figure 1c−f were 30 nm tall nanoposts formed using e-beam evaporation of 1 nm thick chromium and 30 nm thick gold, followed by the process of lift-off. The encapsulated structures shown in Figure 1b would otherwise inhibit imaging. In order to access the real geometry of our pixels and obtain a better analysis of the deposited structure and material, we performed a cross-sectional cut of the nanostructures using focused ion beam milling and SEM imaging. This cut created a "window" beneath the nanostructures, revealing the cross-sectional profile and different layers of the pixel, as shown in Figure 1h,j. Note that the conductive carbon paint and platinum layers are routinely added prior to the SEM imaging and FIB milling to circumvent charging of the sample and as a protective layer. The cross-sectional images in Figure 1h,j show that gaps exist between the sidewall of the PMMA and the deposited metal and that the cross sections of the metal nanostructures have a tilted sidewall profile with rounded tops. These are likely due to the slightly overhang nanostructures in PMMA that might have developed during the metal deposition process. Note that the unprotected side of silver has formed a noticeably thick layer of oxide/sulfide that is of a darker appearance than silver. This layer was not observed on the side in contact with PMMA/SiO_2, suggesting that the deterioration of the metal occurs on the exposed side and that PMMA/SiO_2/glass coatings are effective in preventing the deterioration of silver. The subsequent nanoposts and nanopits are narrower at the top and base of the pixel respectively and could lead to optical responses that are different from the intended design. These air gaps and geometry deviations from the intended designs have been taken into consideration in our simulations.

Preliminary experiments into these color pixels studied nanostructures arranged in a square array. However, increasing the width and pitch sizes in this configuration will result in individual square pixels touching their neighboring structures without gaps in-between structures to form post or pit geometries. Conversely, employing a checkerboard pattern, as shown in Figure 1d−g, ensures a perpetual gap between adjacent squares. This enables the systematic study of the evolution of isolated to conformal structures, where small width and pitch sizes form isolated post/pits and large width and pitch sizes form connected post/pits.

Bright-field optical images (Figure 2a,b) and reflection spectra measurements (Figure 2c,d) were obtained to investigate the optical responses of the fabricated color pixels. Structural widths *d* and pixel pitch *p* were systematically varied from 50−400 nm in 10 nm increments as depicted along the *y* and *x*-axes in the color palettes to investigate the full range of colors that can be achieved for each geometry. The arrays along the diagonal edge consist of protrusions that have just touched at the corners to form arrays of nanopits in a checkerboard configuration. The sudden color change between the patches at the diagonal and in the column right before it, is an indication

DOI: 10.1021/acsphotonics.6b00099
ACS Photonics 2016, 3, 1000−1009

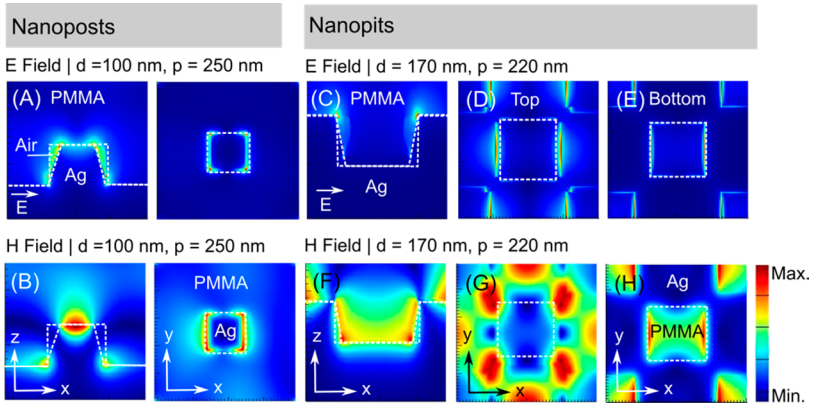

Figure 3. Simulated electric and magnetic field enhancement plots for color pixels comprising nanoposts and nanopits under normal illumination at respective wavelengths of 475 and 539 nm. Field plots for pixels composed of (a, b) 100 nm wide nanoposts, spaced 250 nm apart (Figure 2c) and (c, d) 170 nm wide nanopits spaced 220 nm apart (Figure 2d). We study the (a) electric and (b) magnetic fields at a distance of 2.0 nm nm above the bottom surface of the nanopost. The (c, d, e) electric and (f, g, h,) magnetic field plots at 2.0 nm above the (d, g) top and (e, h) bottom of the nanopit. In the case of the nanopits, we study the (e) electric and (f) magnetic fields at a distance of 2.0 nm above the top and bottom surfaces of the nanopit.

of the change from capacitive to inductively coupled plasmon modes.[34,35]

For the range of structural dimensions chosen, nanoposts exhibit color for a wide range of width and pitch sizes from approximately <100 nm to >140 nm. In stark contrast, nanopits exhibit color only for width and pitch sizes >140 nm, with most arrays appearing colorless. It should be noted that the swatches on the diagonal edge of both nanopost and nanopit palettes are identical in color. This is a result of the checkerboard pattern layout in the palettes of increasing pitch along the diagonal edge. From the color palettes in Figure 2a,b, we observe similar colors that can be grouped into vertical "columns" for the nanoposts, and horizontal "rows" for the nanopits, depicting a color-sensitivity to structure size and pitch, respectively. In Figure 2a, different "hues" of colors generated by pixels are tuned by varying the widths of the posts where yellow, pink, gray-green, and orange colors are exhibited in the vertical columns. As the width of the nanoposts increases, the local resonances exhibit a redshift due to retardation effects, with the wavelength increasing by ∼16 nm for every 10 nm increase in width. This retardation can be seen as a modification to the electrostatic approximation that works for deep subwavelength particles, which takes into consideration reradiation of light, and the fact that the top and bottom of the nanostructures are not experiencing the same phase of the electric field excitation. Without retardation, that is, with the electrostatic approximation of Mie, no wavelength shift will be observed with increasing particle size. Colors created from the nanoposts are thus determined almost entirely by the structural size and arise from localized plasmon resonances.

Color "tones", however, are tuned by varying the pixel pitch (i.e., different shades of pink are obtained within each column for approximately 100 nm < d < 130 nm). In our previous work on isolated nanodisks, we observed that similar shades of colors are generated for pixels with the same fill factor (defined here as d/p).[11] Here, an increase or decrease in the pixel pitch changes the fill factor. This subsequently modulates the amplitude of the color spectra and manifests as a tonal change in color. For example, a decrease in pitch size correlates to an increase in the areal density of color elements. This should, in turn, generate a more "vibrant" tone of the same color[10,11,13] as we move down the columns. At pitch p = 100 nm for a structural width d = 130 nm, the fill factor is 4× greater than the same structure size at p = 400 nm. We note that the color intensity produced by the pixels can be quantified through the magnitude of the reflectance shown in its optical spectra (Figure 2c,d). That is, the smaller the magnitude of the reflectance, the "fainter" the color intensity. From Figure 2a, however, the increase in color intensity is observed to be unexpectedly subtle. The color intensity increases only slightly as the pitch is decreased from 400 nm to ∼200 nm; thereafter, the color intensity decreases as the pitch is decreased from 200 to 50 nm. This deviation from anticipation could be attributed to an incomplete filling of metals for smaller pitch sizes. The actual profile of structures might not be as drawn schematically, as the metal filling could be tapered due to sidewall deposition and shadowing effects. This effect could have led to the incomplete filling of metal into the patterns, which would be a topic for further study.

In terms of spectral tunability, the opposite is true for nanopits where colors generated are tuned by the pixel period. We hypothesize at this point; the nanopits support surface plasmon polaritons (SPP) modes and not localized surface plasmons (LSP) modes as they show more of a dependence on pitch and less on nanopit size. This is reminiscent of how SPPs are excited in hole-aperture arrays in enhanced transmission experiments.[36] Here, yellow, pink, gray-green, and orange colors are exhibited in the horizontal rows, whereas the tones are tuned by varying the widths of the nanopits as shown in Figure 2b. It can also be observed that while similar hues of colors are obtained from the nanopits (i.e., yellow, pink, gray-green, orange), the color tones generated, however, are far fewer in comparison to those for the nanoposts. Such a parameter-dependent spectral tunability agrees with what has been observed in plasmonic nanoantennas versus hole apertures.[1] For example, resonators comprising isolated structures such as disks or rods frequently employed for making reflective color elements are tuned by varying the physical dimensions[3,10−12] of the individual resonators themselves (i.e., diameter of disk, ellipse, or length of grating). Conversely, complementary structures of holes (circular or cross-shape apertures) perforated in metal films typically used for producing transmissive color filters[2,4,5,21] are tuned through variation of the structural periodicity[4,5,21] with a weaker dependence on the size of the holes.

DOI: 10.1021/acsphotonics.6b00099
ACS Photonics 2016, 3, 1000−1009

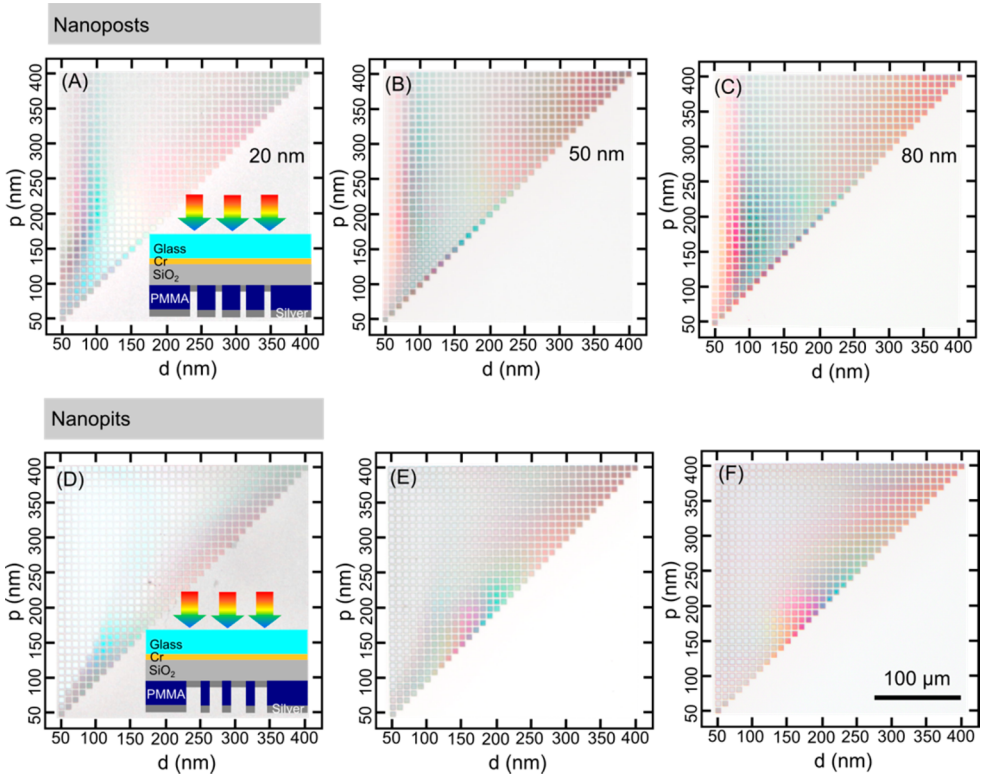

Figure 4. Chromatic modulation from isolated antennas to conformal nanoposts and pits under reflective illumination. Optical micrographs for arrays of nanopatterns comprising (a–c) nanoposts and (d–f) nanopits with varying metal thicknesses of 20–80 nm in 30 nm increments.

Color variations for selected swatches are verified by experimental and simulated reflection spectra shown in Figure 2c,d. For both types of pixels investigated, experimental spectra show comparable trends and demonstrated qualitative agreement with FDTD simulations. A red-shift in the resonances, in the form of spectral dips, can be observed for increasing widths for the nanoposts (Figure 2c) and increasing pitch size for the nanopits (Figure 2d). In the case of the nanoposts, the red-shift in spectra is similar to previous work on isolated nano-antennas[10−12] and shows consistency with the trend observed for gold/silver nanodisks.

Electric and magnetic field enhancement plots at the spectral dips for selected color pixels are simulated to understand the resonant modes. Here, pixel resonances are observed at the dips in the reflection spectra corresponding to light absorption in the metal nanoposts.[11] Field plots for pixels composed of (a, b) 100 nm wide posts, at a wavelength of 550 nm, spaced 250 nm apart (Figure 2c) and (c, d) 170 nm wide pits, at a wavelength of 560 nm spaced 220 nm apart (Figure 2d) are shown in Figure 3.

In the case of the nanoposts, the fields flow around a metallic antenna and would thus, exhibit particle-like resonance behaviors as observed in Figure 3a,b. According to Babinet's principle, the opposite holds true for the nature of the mode and the optical response in the case of the inverse structures of nanopits. For example, the electric field in the nanopits in Figure 3d resemble that of the magnetic field of the nanoposts in Figure 3b, and the magnetic field of the nanopits in Figure 3g show similarities to the electric field of the nanoposts in Figure 3a. As such, the modes for the nanopits are indeed observed to be dissimilar to the nanoposts, producing electric and magnetic fields at different interfaces. In the case of the nanoposts depicted in Figure 3a,b, the mode is shown to be caused by a LSP resonance, where the charges are antisymmetrically distributed about the *y*-axis of the structure, which is perpendicular to the axis of polarization.[33] The top surface of the nanopost has net positive charges on one-half and negative charges on the other, whereas the surface of the silver substrate has the opposite configuration, where the distribution of charges is reversed at the base of the protrusion. Subsequently, energy is stored in the form of a strong electric field parallel to the top surface of the protrusion, in the case of the nanopits, and at the bottom corners of the nanopits.[33] Electric fields form in the *xz*-plane between the substrate and the circumference of the top surface of the nanopost. Magnetic fields also form in the *y*-direction due to the changing electric fields and are located above the top surface and at the bottom edges of the protrusions. These field distributions promote the absorption of light at the asperities of the profile. With energy trapped in this resonance mode, a dip forms in the reflectance spectrum at the resonance wavelength.

To investigate the differences in colors generated from an all-metal surface from that of isolated antennas,[10−12] we study the chromatic modulation as the color elements are varied from arrays of isolated antennas to one composed of connected nanoposts and nanopits. To achieve these structures, the thickness of silver is increased from ∼20 nm up to the thickness of the PMMA film, that is, ∼80 nm. When the "nanopost" arrays are coated with a metal film only tens of nanometers thick, the resultant structure comprises arrays of metal nanosquares on SiO_2, that is, within the PMMA holes, and a perforated metal film on the PMMA surface. These structures are similar to the previously studied electrically "isolated" pixels (Figure 4). At 80 nm thickness, the structures are closer to being conformal, likely with nanogaps between the metal on PMMA and on SiO_2. As the thickness of the metal coating is

DOI: 10.1021/acsphotonics.6b00099
ACS Photonics 2016, 3, 1000−1009

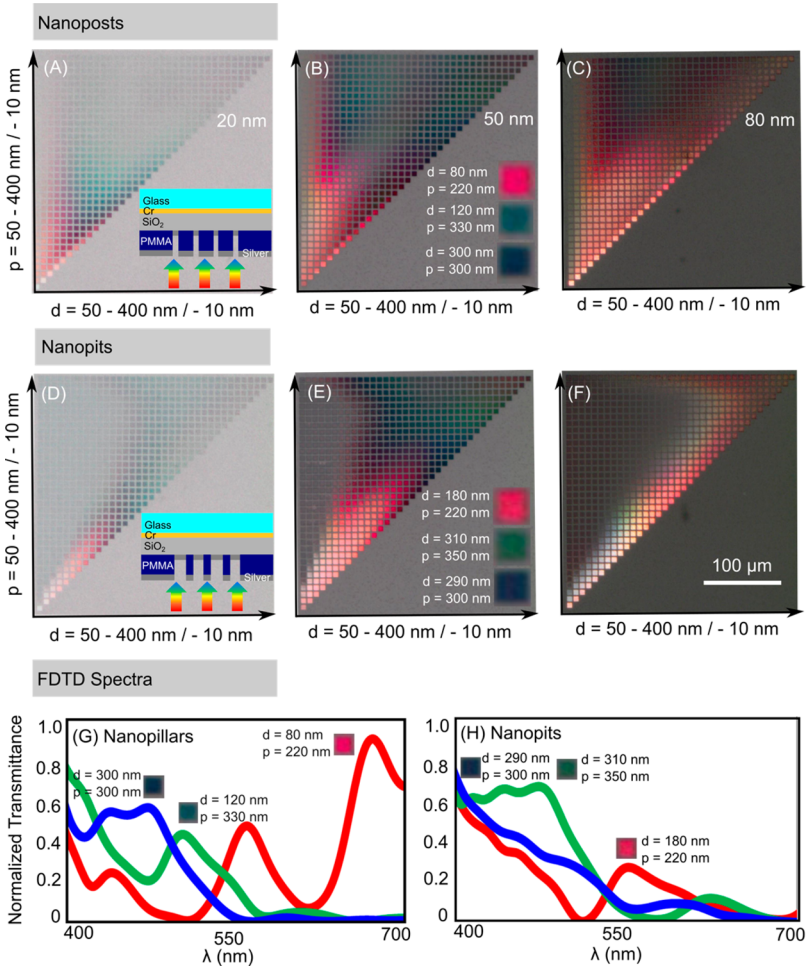

Figure 5. Chromatic modulation from isolated antennas to conformal nanoposts and nanopits under transmissive illumination. Optical micrographs for arrays of nanopatterns comprising (a–c) nanoposts and (d–f) nanopits with varying metal thicknesses of 20–80 nm in 30 nm increments. Inset: selected color swatches from the color palettes for metal thicknesses of 50 nm. Simulated reflection spectra for selected color swatches of (g) nanoposts and (h) nanopits under normal illumination.

increased to hundreds of nanometers, the metal layers on the bottom of the pits and the top of the pillars connect to form a conformal layer of metal to create the nanoposts and pits such as in the schematic shown in Figure 1b.

Figure 4 depicts the optical micrographs for arrays of (a–c) nanoposts and (d–f) nanopits with varying silver thicknesses of 20, 50, and 80 nm under reflective illumination (light collection from the side of the glass substrate). In the case where the metal film coating the nanopost is thin, that is, tens of nanometers thick (i.e., 20 nm), the range of colors generated is narrow. Only a narrow range of colors, such as gray, pink and green can be discerned in the palette. As the film thickness increases, the range of colors, as well as the vibrancy increase. For example, at a metal thickness of 80 nm, yellow, red, pink, green, and orange colors can be observed in the arrays of nanoposts (Figure 4c). A similar improvement in color is observed in the nanopits (Figure 4f) with increasing metal thickness. The optical behavior of these all-metal color elements can be considered analogous to "subtractive colors",[33] colors that are generated through the absorption of light of specific wavelengths and reflection of other wavelengths. In this regard, the increased color range and vibrancy could be attributed to the increased amount of silver deposited, which acts as the absorbing material at resonance and provides a reflective surface off resonance.

Optical micrographs for both nanoposts and nanopits also exhibit colors under transmissive light illumination as shown in Figure 5. In the case of a thinner metal film (~20 nm), colors are generated for swatches closer to the bottom left of the palette—corresponding to structures with smaller dimensions and pitch sizes. As the metal thickness increases to ~50 nm, vibrant colors (e.g., beige, purple-pink and green) are observed for both nanoposts and nanopits. As expected, less light is transmitted at a metal thickness of 80 nm, resulting also in a reduction in the range of colors produced. It is interesting to note that a near-white color is produced for smaller dimensions and pitch sizes for the nanopits (Figure 5f), indicating a broadband transmission.

To have a closer look at the colors produced for the case where the metal is 50 nm, transmission spectra are simulated for selected red, green, and blue color swatches (color swatches shown in Figure 5b,e) in Figure 5g,h. The resonance peaks in the simulated spectra demonstrate qualitative agreement with what one would expect for such colors within the visible spectrum. It can also be noted that the nanoposts exhibit superior transmission of up to simulated value of ~0.09 as compared to the nanopits. Interestingly, more obvious color

DOI: 10.1021/acsphotonics.6b00099
ACS Photonics 2016, 3, 1000–1009

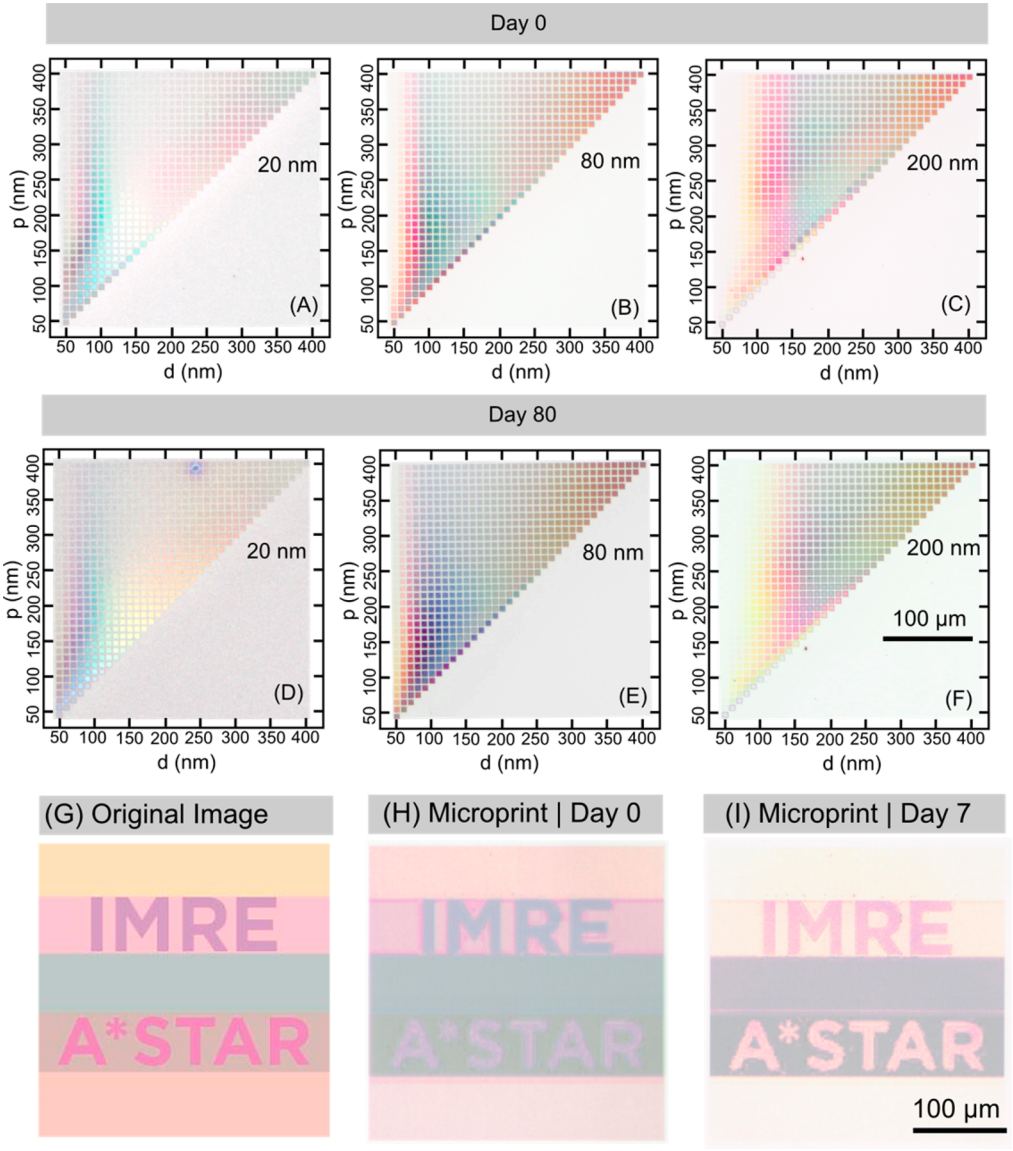

Figure 6. Oxidation and sulphidation effects on plasmonic color palettes and a plasmonic microprint. Optical micrographs for connected arrays of nanoposts with varying metal thicknesses of (a) 20 nm (b) 80 nm, and (c) 200 nm on day 0 and day 80 postmetallization (d–f). (g) MATLAB-generated original image; optical images of the plasmonic microprint on (h) day 0 and (i) day 7 postmetallization.

changes were observed for different metal thicknesses when viewed in transmission than reflection. For example, in Figure 5e, shades of pink, red, purple, and green are exhibited by arrays coated with 50 nm of metal; a substantially different palette of pastel yellows and pinks are observed when the metal thickness is increased to 80 nm in Figure 5f. In all cases under reflective and transmissive illumination, color tuning trends for the structures are consistent with their fully conformal counterparts where modulation occurs through variation of structure dimensions and pitch for the nanoposts and nanopits, respectively. In particular, the colors exhibited in transmission are shown to be more vibrant compared to their reflective counterparts. The structures coated with thinner layers of metal (i.e., 50 nm) generate vibrant colors under transmissive illumination and could possibly be employed for use as transmissive filters.

As a test of the encapsulation layer coating the color elements for inhibiting the effects of oxidization and sulphidation, the color palettes shown in Figures 2 and 4 were imaged again 80 days postfabrication. Note that the encapsulation refers to the fact that the silver nanostructures are enclosed between the bulk silver, PMMA, SiO_2, and glass material layers, as shown in Figure 1b. Figure 6 shows the optical micrographs for connected arrays of nanoposts with varying metal thicknesses of (a, d) 20 nm, (b, e) 80 nm, and (c, f) 200 nm on the day of fabrication (day 0) and 80 days after (day 80). Given that silver is known to deteriorate in a matter of days due to sulphidation, it is remarkable that colors were still visible after 80 days. We note that color changes occur between day 0 and day 80, particularly so for the metal thickness of 20 nm, as anticipated because of the lack of complete encapsulation given the thin metal layer. In the case where the metal layer is 80 nm, the environmental degradation has imparted a blue tint to the color swatches (Figure 6e) that were originally green (Figure 6b). Details of the color degradation in these embedded structures are topics for further detailed research. We hypothesize that the color shifts are due to surface deterioration, which leads to a smaller effective

DOI: 10.1021/acsphotonics.6b00099
ACS Photonics 2016, 3, 1000–1009

volume of the nanostructures. As the metal thickness increases to ~200 nm, we observe that the encapsulation layer acts to preserve the colors generated where minimal color change can be observed. At this metal thickness, the color elements are completely sandwiched between the back-end of the metal film, the dielectric layer, and the SiO_2 spacer layer. Thus, embedding the nanostructures with our material stack only minimizes but does not prevent degradation of silver.

The all-metallic array of nanoposts was next used in creating a simple microimage based on experimentally obtained color palettes shown in Figure 2a. The digital image was first input into a MATLAB script that performed the closest RGB color match for individual pixels in the image, to color swatches in the palette. This generated a layout of nanodisks with structural dimensions and pitch used for the background color and foreground text in the range of 90−400 nm. The original MATLAB-generated image is shown in Figure 6g; the optical images of the plasmonic microprint on day 0 and day 7 postfabrication are shown in Figure 6h and i, respectively. In Figure 6h, the fabricated plasmonic microprint on day 0 shows decent agreement with the original image, with accurate replication of the background color and acronyms in the foreground. We note that, given that these colors are very sensitive to the nanostructure size, the slight deviation of color from the input image is likely to be due to imperfect fabrication, which led to a different pixel width and, hence, color. In spite of the demonstration of color preservation in Figure 6i, we note that some oxidation effects resulted in perceivable color changes in the microprint. While not an intended outcome, this color change could instead, be employed as a means of a color timestamp to indicate the approximate age of the microprint from the time of metallization. The addition of another encapsulation layer, such as PMMA or an epoxy on top of the bulk silver layer may impart further protection that could considerably increase the lifetime of the colors. Regardless, colors in the microprint have been preserved to a large extent and can still be observed in the microprint. Interestingly, the letters "A*STAR" become more visible with the age of the sample.

We presented the generation of colors from an all-metal, optically thick film comprising nanometric nanoposts and nanopits. Results show generally that nanoposts support LSP resonances that dependent on post size, while nanopits arrays support standing SPP waves that are dependent on pitch size. Significant color shifts were observed when isolated nanoposts merge to form nanopits arrays. We showed that these structures generate surprisingly vibrant colors when viewed in transmission; despite its modest absolute peak transmittance of ~10%. Additionally, the work reported here sets the stage for further studies, for example, into the sudden shift in resonance close to the diagonals in the color palettes which could be useful in color switching applications. The demonstration of a simple color microprint indicates that such color elements could provide a flexible alternative to dye-based colorants. The architecture of these designs provides useful advantages for commercial implementation including nonreliance on vacuum-based metallization, pixels that are robust against degradation from exposure to atmospheric conditions, and embedded features that are resistant to scratches. These color elements have potential utility in direct color printing onto metal surfaces (e.g., for coins and other metal finishes), and will also render the processes for fabricating plasmonic color pixels on plastic films economically feasible. Scale-up mass-volume methods such as nanoimprint lithography can also be employed to bring these color elements closer to industrially relevant production. Furthermore, due to the structure's architecture, the plasmonic metal layer is inherently protected as it will be encapsulated between itself and the substrate—making way for a "self-protecting", ultradurable color element.

METHODS

Electron Beam Lithography (EBL). Color information in the microprints was encoded in the form of nanostructure dimension and position by use of MATLAB (The Mathworks Inc.) for fabrication in EBL. For both nanoposts and nanopits, Corning glass substrates were deposited with a 1 nm layer of chromium to circumvent charging during lithography; a 100 nm SiO_2 spacer layer was deposited to reduce plasmon coupling with the pixel layer. To write both structures, positive-tone electron beam resist PMMA (950 K molecular weight, MicroChem Corp., 1.67% in anisole) was spin-coated at 3000 rpm to a thickness of ~80 nm. Baking of the resist was performed at 180 °C for 2 min. Computer-generated pattern layouts were in-put into the lithography system for writing. EBL was performed using an Elionix ELS-7000 EBL system (Elionix Inc.) with an accelerating voltage of 100 kV and a beam current of 200 pA. A write field of 150 μm × 150 μm, with an exposure step size of 2.5 nm, was employed. No proximity-effect correction was performed for any exposure. Unexposed regions of PMMA resist were removed by immersing the samples in a 1:3 MIBK/IPA developer at room temperature for 50s. Finally, the samples were blow-dried with a steady stream of N_2. It should be noted that no lift-off was performed so as to maintain the encapsulating layer between the metal features and SiO_2 spacer layer.

Metal Deposition. Metal deposition was performed using an electron beam evaporator (Explorer Coating System, Denton Vacuum Inc.) at a working pressure of ~1×10^{-6} Torr. A 200 nm thick layer of silver was deposited onto the samples at the rate of 5.0 Å/s. During the evaporation process, the sample chamber was kept at a constant temperature of 20 °C and the sample holder was rotated at 50 rpm to maintain uniform deposition.

Optical Measurements. Bright-field optical microscopy and reflection spectra measurements of the color palettes were performed to investigate the optical responses of the fabricated structures. Extinction spectrometry in reflection mode was achieved using a UV−visible-NIR microspectrophotometer (CRAIC Technology Inc.) at normal incidence with a 75 W broadband xenon source. White light was passed through an objective lens (36× 0.5 NA) to illuminate the samples at normal incidence to the substrate. Using a variable aperture set to a detecting area of 7.1 μm × 7.1 μm, reflected light (λ = 400−800 nm) was collected through the same objective and back into the spectrometer and CCD camera. Optical images in reflection and transmission were captured using a conventional upright bright-field microscope (Olympus MX61, Olympus Inc.) equipped with a digital camera (SC30 Olympus). Images of samples were magnified by an objective lens (Olympus Mplan 50× 0.8 NA) in order to observe the different colors generated. Postprocessing steps (background normalization) for the optical images were performed using ImageJ (NIH, Maryland, U.S.A.).

DOI: 10.1021/acsphotonics.6b00099
ACS Photonics 2016, 3, 1000−1009

NUMERICAL SIMULATIONS

The optical responses of the color pixels, the reflectance, transmittance, and electric/magnetic field distributions, were modeled using a commercial finite-difference time domain (FDTD) solver (Lumerical FDTD Solutions). The simulated structure was a periodic array of 13 identical posts/pits with the required lateral dimensions and heights. The sides and corners of the posts/pits were rounded with a radius of curvature of 10 nm. A mesh size of 2.5 nm was used to ensure high accuracy. The refractive index data for silver were taken from Palik,[37] while a constant refractive index of 1.3 was used for the PMMA and glass layers. A normally incident plane wave with linear polarization parallel to the sides of the posts/pits was used as the source, while the reflected power was measured using a field monitor placed above the source. Perfectly matched layer (PML) boundaries were used for all sides of the simulation region.

AUTHOR INFORMATION

Corresponding Author

*E-mail: joel_yang@sutd.edu.sg.

Notes

The authors declare no competing financial interest.

ACKNOWLEDGMENTS

The authors would like to acknowledge funding support from the Institute of Materials Research and Engineering, Agency for Science, Technology and Research (A*STAR), A*STAR Joint Council Office (Grant No. 14302FG092) and the Singapore University of Technology and Design (SUTD). The authors would like to thank Henri Lezec for useful discussions. The authors also thank J. Deng, V. Lim, and S. L. Teo from the Institute of Materials Research and Engineering for technical assistance.

REFERENCES

(1) Tan, S. J.; Goh, X. M.; Wang, Y. M.; Yang, J. K. W. Y.; Teng, J. Engineering Plasmonic Colors In Metal Nanostructures. *J. Mol. Eng. Mater.* **2014**, *02*, 1440011.

(2) Ellenbogen, T.; Seo, K.; Crozier, K. B. Chromatic Plasmonic Polarizers for Active Visible Color Filtering and Polarimetry. *Nano Lett.* **2012**, *12*, 1026−1031.

(3) Xu, T.; Wu, Y.; Luo, X.; Guo, L. J. Plasmonic Nanoresonators for High-Resolution Colour Filtering and Spectral Imaging. *Nat. Commun.* **2010**, *1*, 59.

(4) Zeng, B.; Gao, Y.; Bartoli, F. J. Ultrathin Nanostructured Metals for Highly Transmissive Plasmonic Subtractive Color Filters. *Sci. Rep.* **2013**, *3*, 2840.

(5) Shrestha, V. R.; Lee, S.; Kim, E.; Choi, D. Aluminum Plasmonics Based Highly Transmissive Polarization- Independent Subtractive Color Filters Exploiting a Nanopatch Array. *Nano Lett.* **2014**, *14*, 6672−6678.

(6) Kaplan, A. F.; Xu, T.; Jay Guo, L. High Efficiency Resonance-Based Spectrum Filters with Tunable Transmission Bandwidth Fabricated Using Nanoimprint Lithography. *Appl. Phys. Lett.* **2011**, *99*, 143111.

(7) Sun, L. B.; Hu, X. L.; Zeng, B.; Wang, L. S.; Yang, S. M.; Tau, R. Z.; Fecht, H. J.; Z, D. X.; J, J. Z. Effect of Relative Nanohole Position on Colour Purity of Ultrathin Plasmonic Subtractive Colour Filters. *Nanotechnology* **2015**, *26*, 305204.

(8) Ye, M.; Sun, L.; Hu, X.; Shi, B.; Zeng, B.; Wang, L.; Zhao, J.; Yang, S.; Tai, R.; Fecht, H.-J.; Jiang, J.-Z.; Zhang, D.-X. Angle-Insensitive Plasmonic Color Filters with Randomly Distributed Silver Nanodisks. *Opt. Lett.* **2015**, *40*, 4979.

(9) Zheng, B. Y.; Wang, Y.; Nordlander, P.; Halas, N. J. Color-Selective and CMOS-Compatible Photodetection Based on Aluminum Plasmonics. *Adv. Mater.* **2014**, *26*, 6318−6323.

(10) Tan, S. J.; Zhang, L.; Zhu, D.; Goh, X. M.; Qiu, C.-W.; Yang, J. K. W. Wide-Range Plasmonic Palette for Photorealistic Color Printing with Aluminum Nanostructures. *Nano Lett.* **2014**, *14*, 4023−4029.

(11) Kumar, K.; Duan, H.; Hegde, R. S.; Koh, S. C. W.; Wei, J. N.; Yang, J. K. W. Printing Colour at the Optical Diffraction Limit. *Nat. Nanotechnol.* **2012**, *7*, 1−15.

(12) Goh, X. M.; Zheng, Y.; Tan, S. J.; Zhang, L.; Kumar, K.; Qiu, C.-W.; Yang, J. K. W. Three-Dimensional Plasmonic Stereoscopic Prints in Full Colour. *Nat. Commun.* **2014**, *5*, 5361.

(13) Clausen, J.; Højlund-Nielsen, E.; Christiansen, A.; Yazdi, S.; Grajower, M.; Taha, H.; Levy, U.; Kristensen, A.; Mortensen, N. Plasmonic Metasurfaces for Coloration of Plastic Consumer Products. *Nano Lett.* **2014**, *14*, 4499−4504.

(14) Roberts, A. S.; Pors, A.; Albrektsen, O.; Bozhevolnyi, S. I. Subwavelength Plasmonic Color Printing Protected for Ambient Use. *Nano Lett.* **2014**, *14*, 783−787.

(15) Xue, J.; Zhou, Z.-K.; Wei, Z.; Su, R.; Lai, J.; Li, J.; Li, C.; Zhang, T.; Wang, X.-H. Scalable, Full-Colour and Controllable Chromotropic Plasmonic Printing. *Nat. Commun.* **2015**, *6*, 8906.

(16) Li, Z.; Clark, A. W.; Cooper, J. M. Dual Color Plasmonic Pixels Create a Polarization Controlled Nano Color Palette. *ACS Nano* **2016**, *10*, 492−498.

(17) Olson, J.; Manjavacas, A.; Liu, L.; Chang, W.-S.; Foerster, B.; King, N. S.; Knight, M. W.; Nordlander, P.; Halas, N. J.; Link, S. Vivid, Full-Color Aluminum Plasmonic Pixels. *Proc. Natl. Acad. Sci. U. S. A.* **2014**, *111*, 14348−14353.

(18) Yang, Y.; Wang, W.; Moitra, P.; Kravchenko, I. I.; Briggs, D. P.; Valentine, J. Dielectric Meta-Reflectarray for Broadband Linear Polarization Conversion and Optical Vortex Generation. *Nano Lett.* **2014**, *14*, 1394−1399.

(19) Zhang, J.; Ou, J.-Y.; MacDonald, K. F.; Zheludev, N. I. Optical Response of Plasmonic Relief Meta-Surfaces. *J. Opt.* **2012**, *14*, 114002.

(20) Wu, Y.-K. R.; Hollowell, A. E.; Zhang, C.; Guo, L. J. Angle-Insensitive Structural Colours Based on Metallic Nanocavities and Coloured Pixels beyond the Diffraction Limit. *Sci. Rep.* **2013**, *3*, 1194.

(21) Inoue, D.; Miura, A.; Nomura, T.; Fujikawa, H.; Sato, K.; Ikeda, N.; Tsuya, D.; Sugimoto, Y.; Koide, Y. Polarization Independent Visible Color Filter Comprising an Aluminum Film with Surface-Plasmon Enhanced Transmission through a Subwavelength Array of Holes. *Appl. Phys. Lett.* **2011**, *98*, 093113.

(22) Ahn, S. H.; Guo, L. J. Large-Area Roll-to-Roll and Roll-to-Plate Nanoimprint Lithography: A Step toward High-Throughput Application of Continuous Nanoimprinting. *ACS Nano* **2009**, *3*, 2304−2310.

(23) Feuerstein, A.; Mayr, M. High Vacuum Evaporation of Ferromagnetic Materials, a New Production Technology for Magnetic Tapes. *IEEE Trans. Magn.* **1984**, *20*, 51−56.

(24) Sauvage-Vincent, J.; Tonchev, S.; Veillas, C.; Reynaud, S.; Jourlin, Y. Optical Security Device for Document Protection Using Plasmon Resonant Transmission through a Thin Corrugated Metallic Film Embedded in a Plastic Foil. *J. Eur. Opt. Soc.* **2013**, *8*, 13015.

(25) Duempelmann, L.; Luu-Dinh, A.; Gallinet, B.; Novotny, L. Fourfold Color Filter Based on Plasmonic Phase Retarder. *ACS Photonics* **2015**, *9*, 12383.

(26) Duempelmann, L.; Casari, D.; Luu-Dinh, A.; Gallinet, B.; Novotny, L. Color Rendering Plasmonic Aluminum Substrates with Angular Symmetry Breaking. *ACS Nano* **2015**, *9*, 12383−12391.

(27) Perednis, D.; Gauckler, L. J. Thin Film Deposition Using Spray Pyrolysis. *J. Electroceram.* **2005**, *14*, 103−111.

(28) Kapur, N.; Hewson, R.; Sleigh, P. A.; Summers, J. L.; Thompson, H. M.; Abbott, J. S. A Review of Gravure Coating Systems. *Convert. e-Print* **2011**, *1*, 56−60.

(29) Zhang, J.; Ou, J.-Y.; Papasimakis, N.; Chen, Y.; MacDonald, K. F.; Zheludev, N. I. Continuous Metal Plasmonic Frequency Selective Surfaces. *Opt. Express* **2011**, *19*, 23279−23285.

DOI: 10.1021/acsphotonics.6b00099
ACS Photonics 2016, 3, 1000−1009

(30) Knight, M. W.; Liu, L.; Wang, Y.; Brown, L.; Mukherjee, S.; King, N. S.; Everitt, H. O.; Nordlander, P.; Halas, N. J. Aluminum Plasmonic Nanoantennas. *Nano Lett.* **2012**, *12*, 6000−6004.
(31) Oates, T. W. H.; Losurdo, M.; Noda, S.; Hinrichs, K. The Effect of Atmospheric Tarnishing on the Optical and Structural Properties of Silver Nanoparticles. *J. Phys. D: Appl. Phys.* **2013**, *46*, 145308.
(32) Mcmahon, M. D.; Lopez, R.; Meyer, H. M.; Feldman, L. C.; Haglund, R. F. Rapid Tarnishing of Silver Nanoparticles in Ambient Laboratory Air. *Appl. Phys. B: Lasers Opt.* **2005**, *80*, 915−921.
(33) Ng, R. J. H.; Goh, X. M.; Yang, J. K. W. All-Metal Nanostructured Substrates as Subtractive Color Reflectors with near-Perfect Absorptance. *Opt. Express* **2015**, *23*, 32597.
(34) Duan, H.; Fernández-Domínguez, A. I.; Bosman, M.; Maier, S. a; Yang, J. K. W. Nanoplasmonics: Classical down to the Nanometer Scale. *Nano Lett.* **2012**, *12*, 1683−1689.
(35) Hu, H.; Duan, H.; Yang, J. K. W.; Shen, Z. X. Plasmon-Modulated Photoluminescence of Individual Gold Nanostructures. *ACS Nano* **2012**, *6*, 10147−10155.
(36) Ebbesen, T. W.; Lezec, H. J.; Ghaemi, H. F.; Thio, T.; Wolff, P. A.; Thio, T. Extraordinary Optical Transmission through Sub-Wavelength Hole Arrays. *Nature* **1998**, *86*, 1114−1117.
(37) Palik, E. D. *Handbook of Optical Constants of Solids*; Academic Press, 1998.

DOI: 10.1021/acsphotonics.6b00099
ACS Photonics 2016, 3, 1000−1009